

Light-front wavefunction dependence of the quark recombination and a new prediction on hadron ratios in the fragmentation region

Byungsik Hong^{*}

Department of Physics, Korea University, Seoul 136-701, Korea

Chueng-Ryong Ji[†]

Department of Physics, North Carolina State University, Raleigh, North Carolina 27695

Dong-Pil Min[‡]

School of Physics, Seoul National University, Seoul 151-747, Korea

(Dated: March 21, 2019)

Abstract

We present an extension of the recombination formalism to analyze the effects from the variation of the hadron wavefunctions. The hadron spectra is sensitive to the shape of the wavefunctions. However, when we fit the wavefunction parameters to the physical observables, such as the average charge radius, the final spectra are very similar each other. We discuss our numerical results in comparison with the published PHENIX and STAR data at RHIC. In the hadron spectra, the recombination of thermal partons dominates at intermediate transverse momentum ($P_T = 2 \sim 5$ GeV), and the fragmentation dominates at high P_T (> 5 GeV). The yield ratios and the nuclear modification factors for various hadron species are also estimated and compared to the experimental data. We present a new prediction on \bar{p}/p and K^-/K^+ ratios, including the jet quenching effects to the fragmentation mechanism.

PACS numbers: 25.75.-q, 25.75.Dw, 12.39.-x

^{*}Electronic address: bhong@korea.ac.kr

[†]Electronic address: ji@ncsu.edu

[‡]Electronic address: dpmin@snu.ac.kr

I. INTRODUCTION

Although no one doubt the existence of quarks and gluons, they have not yet been detected individually at the zero temperature. The current vigorous efforts at the Relativistic Heavy Ion Collider (RHIC) and the future plans of the Large Hadron Collider (LHC) may reveal the temperature dependence of the confinement mechanism and the chrial symmetry restoration [1]. The high-energy nuclear collisions compress and heat the heavy nuclei so much that their individual protons and neutrons may overlap and, in addition, a lot of pions may arise to ultimately create the quark-gluon plasma (QGP). The QGP may have existed ten millionths of second after the big bang and created the primordial matter of the universe. The RHIC and the future LHC may yield the QGP in the laboratory. It has been reported that the four experiments at RHIC already obtained distinguished results from the lower energy heavy ion collisions at CERN SPS [2, 3, 4, 5]. The future LHC experiments (ALICE as well as CMS and ATLAS) would require theoretical predictions at the 30-fold energy increase from the RHIC.

Among many others, the effects from the jet quenching and the bulk hadronization may be regarded as the important new results. Especially, the elliptic flow analysis revealed that the differential second-harmonic Fourier moment (v_2) of the azimuthal distribution with respect to the reaction plane had a remarkable saturation property in the intermediate transverse momentum (P_T) range between 2 and 6 GeV for all hadrons including multi-strange baryons. This saturation effect and eventual decrease of v_2 at high P_T has been qualitatively interpreted to be the result of partonic energy loss in an opaque parton system created by nuclear collisions [6, 7]. Furthermore, the estimated v_2 parameter as a function of P_T are scaled by the number of constituent quarks of particles. Together with an enhanced proton production in the intermediate P_T region, this agreement has been taken seriously as one piece of evidence for the quark recombination process and the presence of partonic collectivity at the early stage of a collision [8, 9, 10, 11, 12, 13].

In this work, we utilize the previous recombination formalism, and extend it to analyze the light-front (LF) wavefunction dependence in the theoretical predictions from this formalism. Typical forms of the LF wavefunctions such as the Gaussian form and the power-law form are applied to this extended formulation. The numerical results are contrasted to each other, and compared with the available single invariant spectra by PHENIX and STAR for various

mesons and baryons. We also discuss the production ratios of various hadrons, including \bar{p}/p and K^-/K^+ , in the fragmentation region. While we include the jet quenching effects as others do, we get a rather distinguished results compared to the previous ones. For the high P_T regions, we get a dramatic suppression of the antiparticles \bar{p} and K^- compare to the corresponding particles p and K^+ , respectively.

The paper is organized as follows. In Sec. II, we present the recombination formalism which is extended from the previous one to explicitly include the intrinsic transverse momenta of the constituents inside the hadron. Rather than an extensive review of the previous formalism, we focus on what has been extended from the previous model. In Sec. III, we present the numerical results of the P_T spectra for various mesons and baryons to contrast the results between the Gaussian form and the power-law form. The results are compared with the available experimental data from PHENIX and STAR collaborations. We also discuss the production ratios of various hadrons and the nuclear modification factor R_{CP} in this section. Conclusions and discussions follow in Sec. IV.

II. FORMULATION

A. Recombination and Light-Front Wavefunction Dependence

The current data from the RHIC experiments seem to indicate two distinguished mechanisms of hadronization: (1) quark recombination for a rather low and intermediate P_T region and (2) quark fragmentation for a high P_T region. In this section, we present an extension of the recombination formalism to analyze the effects from the variation of the hadron wavefunctions.

Introducing the density matrix $\hat{\rho}$ for the system of partons, the number of quark-antiquark states that one may interpret as mesons is given by

$$N_M = \sum_{ab} \int \frac{d^3 P}{(2\pi)^3} \langle M; P | \hat{\rho}_{ab} | M; P \rangle, \quad (1)$$

where $|M; P\rangle$ is a meson state with the momentum P and the sum is over all combinations of quantum numbers such as flavor, helicity, and color of the valence partons that contribute to the given meson M . Inserting complete sets of coordinates and using the Wigner function

formalism, one can derive the formula for the invariant spectrum of the meson M as follows:

$$\begin{aligned}
E \frac{d^3 N_M}{dP^3} &= C_M \int_{\Sigma} \frac{d^3 R P \cdot u(R)}{(2\pi)^3} \int \frac{d^3 q}{(2\pi)^3} \\
&\quad \times w_a(R; \frac{P}{2} - q) \Phi_M^W(q) w_b(R; \frac{P}{2} + q) \\
&= C_M \int_{\Sigma} \frac{d^3 R P \cdot u(R)}{(2\pi)^3} \int \frac{dx P^+ d^2 \vec{k}_\perp}{(2\pi)^3} \\
&\quad \times w_a(R; x P^+, \vec{k}_\perp) \Phi_M(x, \vec{k}_\perp) w_b(R; (1-x) P^+, -\vec{k}_\perp), \tag{2}
\end{aligned}$$

where $\Phi_M^W(q) = \int d^3 r \Phi_M^W(r, q)$ in the Wigner function formalism and $\Phi_M(x, \vec{k}_\perp) = |\psi_M(x, \vec{k}_\perp)|^2$ using the LF wavefunction of the meson $\psi_M(x, \vec{k}_\perp)$. Here, x and \vec{k}_\perp are the momentum fraction and the respective intrinsic transverse momentum of each parton.

The previous work by Fries and collaborators used a factorized ansatz for the LF wavefunction [8],

$$\psi_M(x, \vec{k}_\perp) = \phi_M(x) \Omega(\vec{k}_\perp), \tag{3}$$

with a longitudinal distribution amplitude $\phi_M(x)$ and a transverse part $\Omega(\vec{k}_\perp)$. However, we note that such factorization ansatz cannot be justified since the LF wavefunction depends on the LF invariant mass of the meson, e.g., $(m_a^2 + \vec{k}_\perp^2)/x + (m_b^2 + \vec{k}_\perp^2)/(1-x)$ (here the meson is composed of parton a and b), and the LF invariant mass cannot be factorized as Eq.(3). Thus, we do not integrate over \vec{k}_\perp in Eq.(2) but leave \vec{k}_\perp explicitly in the formulation.

The usual parton spectrum at a given temperature is given by

$$w_a(R; p) = \gamma_a e^{-p \cdot v(R)/T} \cdot e^{-\eta^2/2\Delta^2} f(\rho, \phi), \tag{4}$$

where $v(R)$ and η are the velocity four vector and the rapidity of the parton a , respectively. In addition, $\gamma_a = \mu_a/T$ is a fugacity factor for each parton species a for which we adopt the results from the statistical analysis for the hadron production at RHIC [14]: the chemical potential μ_a 's are 9, 6.7, and -3.9 MeV for $a = u$ (or d), s , and c , respectively. We assume that the temperature T for hadronization occurs at 175 MeV. The space-time structure of the parton source in Eq.(4) is given by a transverse distribution $f(\rho, \phi)$ and a wide Gaussian rapidity distribution with a width Δ . Also, one may assume $f(\rho, \phi) \approx \Theta(\rho_0 - \rho)$ especially for the analysis of the central collisions. With these assumptions, we find

$$\begin{aligned}
\frac{d^3 N_M}{dP_T^2 dy} \Big|_{y=0} &= C_M M_T \frac{V}{(2\pi)^3} 2\gamma_a \gamma_b I_0 \left[\frac{P_T \sinh \eta_T}{T} \right] \\
&\quad \times \int_0^1 dx \int_0^\infty d^2 \vec{k}_\perp |\psi_M(x, \vec{k}_\perp)|^2 k_M(x, \vec{k}_\perp, P_T), \tag{5}
\end{aligned}$$

where $V = \tau A_T$ (τ is the hadronization time and A_T is the transverse size) is the volume of the parton system and

$$k_M(x, \vec{k}_\perp, P_T) = K_1 \left[\frac{\cosh \eta_T}{T} \left[\sqrt{m_a^2 + (x P_T + \vec{k}_\perp)^2} + \sqrt{m_b^2 + \{(1-x) P_T - \vec{k}_\perp\}^2} \right] \right]. \quad (6)$$

We note that the particular combination of P_T and \vec{k}_\perp for each constituent in Eq.(6) is consistent with the boost invariance of k_M in light-front dynamics. Extension to the baryon case is straightforward. In the following analysis, we take V as a free parameter to fit all invariant spectra of hadrons simultaneously for a given collision centrality.

With this extension, we can now explicitly include the effect from the intrinsic transverse momentum of each parton, and vary the form of the LF wavefunction such as the Gaussian form and the power-law form [15]. In this analysis, we use the following typical LF wavefunctions for mesons (the extension to baryons should be simple) and contrast the results between the two:

$$\psi_{Gaussian}(x, \vec{k}_\perp) = \exp \left[-\left(\frac{m_a^2 + \vec{k}_\perp^2}{x} + \frac{m_b^2 + \vec{k}_\perp^2}{1-x} \right) / \beta^2 \right], \quad (7)$$

and

$$\psi_{Power-law}(x, \vec{k}_\perp) = 1 / \left[\frac{m_a^2 + \vec{k}_\perp^2}{x} + \frac{m_b^2 + \vec{k}_\perp^2}{1-x} + \alpha^2 \right]^n, \quad (8)$$

where β , α , and n are the parameters that can be fixed from the physical observables such as the size and the mass spectrum of meson, etc.. Just to illustrate how the LF wavefunctions look like, we plot $\psi_{Gaussian}(x, \vec{k}_\perp)$ for different β^2 values in Fig. 1. As expected, the LF wavefunctions are symmetric around $x = 0.5$, if the masses of constituent quark and antiquark are the same for pions ($m_a = m_b = 0.26$ GeV). As β^2 increases, $\psi_{Gaussian}(x, \vec{k}_\perp)$ becomes broader in x as well as in \vec{k}_\perp . When the mass of constituent quark and antiquark are not the same like K and D , $\psi_{Gaussian}(x, \vec{k}_\perp)$'s are clearly skewed in x .

In order to constraint β , α , and n in Eqs. (7) and (8), the average values of \vec{k}_\perp are fixed by the measured average charge radius $\langle r \rangle$ of each hadrons. If the experimental data for $\langle r \rangle$ are not available, we adopt the calculated ones by a relativistic quark model [16, 17]. As an example, $\langle r^2 \rangle = 4.4$ fm 2 for pions, and the corresponding β^2 is 0.825 GeV 2 for $\psi_{Gaussian}$. In addition, the corresponding α^2 and n are 0.5 GeV 2 and 1, respectively, for $\psi_{Power-law}$. The left two panels of Fig. 2 show the comparison of $\psi_{Gaussian}$ and $\psi_{Power-law}$ of pions by using the adjusted wavefunction parameters. They demonstrate

that the LF wavefunctions are very similar in shape when the parameters are determined by some physical observables such as the charge radii of hadrons. However, if we use some arbitrary values for those parameters, the shape of LF wavefunctions can be quite different, which is demonstrated in the lower right panel of Fig. 2.

The importance of the proper choice of the LF wavefunction parameters in the hadron spectra are explained in Fig. 3 for π 's and D 's. The invariant yields of the recombined mesons are quite different for different sets of parameters. However, the hadron yields from the recombination process are quite similar for $\psi_{Gaussian}$ and $\psi_{Power-law}$, once these parameters are fixed by some physical observables (solid vs. dashed lines). In the following analysis, we use only the Gaussian wavefunction with proper β for each hadron.

B. Fragmentation and Jet Quenching

Inclusive hadron production by fragmentation at large momentum transfer can be described well by perturbative quantum chromodynamics (pQCD). In the framework of pQCD, the invariant yield of hadron h with momentum P is given by

$$E \frac{d^3 N_h^{frag}}{dP^3} = \sum_a \int_0^1 \frac{dz}{z^2} D_{a \rightarrow h}(z) E_a \frac{d^3 N_a^{pert}}{dp_a^3}, \quad (9)$$

where the sum runs over all constituent parton species a in h . For the spectrum of parton a with momentum $p_a = P/z$ at midrapidity, we use the parameterization by pQCD:

$$E_a \frac{d^3 N_a^{pert}}{dp_a^3} = \frac{d^2 N_a^{pert}}{2\pi p_{aT} dp_{aT} dy} \Big|_{y=0} = \frac{K}{\pi} \frac{C}{(1 + p_{aT}/B)^\kappa}, \quad (10)$$

where the parameters C , B , and κ are taken from a leading order pQCD calculations [18]. $K = 1.5$ is taken in order to consider higher order corrections approximately [8]. Note that the number of partons in different collision centralities are obtained by scaling the number of binary nucleon-nucleon collisions (N_{coll}) or, equivalently, by the nuclear thickness function (T_{AA}). The probability that parton a fragments into hadron h is taken into account by the fragmentation function

$$D_{a \rightarrow h}(z) = N z^\gamma (1 - z)^\delta, \quad (11)$$

where the numerical values of N , γ , and δ are taken from the parameterization by Kniehl, Kramer, and Pötter [19] for fragmentation of pions, kaons, protons and antiprotons. A

fragmentation function is taken from the work by de Florian, Stratmann and Vogelsang [20].

Finally, the energy loss of energetic partons (so called jet quenching), especially, in central collisions is considered by the following parameterization [21, 22]

$$\Delta p_T(b, p_T) = \epsilon(b) \sqrt{p_T} \frac{\langle L \rangle(b)}{R_A}, \quad (12)$$

where R_A is the radius of nucleus A , $\langle L \rangle(b)$ is the geometrical factor of the overlap zone of two nuclei, and $\epsilon(b)$ is the energy loss parameter of the hot medium with impact parameter b . The detailed functional forms of $\langle L \rangle(b)$ and $\epsilon(b)$ can be found in Ref. [8], but, practically speaking, it is reasonable to assume that $\langle L \rangle(b) \simeq R_A$ and $\epsilon(b) \simeq 0.82 \text{ GeV}^{1/2}$ for the most central collisions as $b \rightarrow 0$.

III. RESULTS

A. Invariant Spectra

Figure 4 shows the numerical results on the invariant spectra of various mesons at midrapidity for central Au + Au collisions at $\sqrt{s_{NN}} = 200 \text{ GeV}$. In Fig. 4, we compare our calculations for the hadron spectra with the published PHENIX and STAR data [23, 24, 25, 26, 27]. The neutral pion spectrum was measured by PHENIX up to 10 GeV in P_T , but lacks data in a low P_T region. In contrary, the charged pions were measured only at low P_T up to 3 GeV with high precision. However, the high P_T spectra of charged pions are expected to be very similar to those of neutral pions. For charged kaons, PHENIX measured up to 2 GeV, and STAR measured up to about 0.7 GeV in P_T . In general, the data by PHENIX and STAR agree quite well in the overlapped phase space except ϕ : the STAR data is about a factor of three larger than the PHENIX data.

In Fig. 4, the dashed and dotted lines represent the model calculations from the recombination and the fragmentation, respectively, and the solid lines are the sum of two contributions. In the π^0 spectra, the two distinguished P_T regions of hadron production are manifest. Although the transient P_T depends on the particle species, the recombination process is dominant between ~ 2 and 5 GeV, and the fragmentation is dominant above 5 GeV. Our calculation is not expected to reproduce the hadron spectra below about 2 GeV in P_T . In such a very low P_T region, the calculation underestimates the experimental data

significantly, implying that other processes like the transverse flow, the secondary decay of hadron resonances, and the binding energy effect become important. Our calculation reproduces the measured meson P_T spectra larger than 2 GeV reasonable well, including the strange mesons. Note that we do not plot the fragmentation contribution for ϕ due to the lack of the fragmentation function.

Figure 5 shows the numerical results on the invariant spectra of baryons at midrapidity for central Au + Au collisions at $\sqrt{s_{NN}} = 200$ GeV. Figure 5 also compares the calculations with the published experimental data with the open circles by PHENIX [24, 28] and the solid triangles by STAR [26, 29, 30]. The left most column of Fig. 5 is for protons and antiprotons; PHENIX and STAR measured up to about 5 and 1.2 GeV, respectively. Note that the published P_T spectra for protons and antiprotons by STAR [26] are about 40 % higher than those by PHENIX [24]. This difference comes from the fact that the contributions from the Λ and Σ^0 decays are removed only for PHENIX. For a fair comparison between the two data sets, the p and \bar{p} spectra by the STAR collaboration are scaled by 0.6 in Fig. 5. After scaling down, the STAR spectra agree quite well with the PHENIX spectra in the overlapped phase space. The present model reproduces the measured proton and antiproton spectra reasonably well. The model also predicts that the transient P_T for baryons from recombination to fragmentation is somewhat higher than that for mesons.

In Fig. 5, the experimental invariant spectra of $\Lambda + \Sigma^0$, Ξ^- , Ω^- , and their antiparticles are for $\sqrt{s_{NN}} = 130$ GeV. But all model calculations are for $\sqrt{s_{NN}} = 200$ GeV because all input parameters of the model calculations are available only for $\sqrt{s_{NN}} = 200$ GeV. Furthermore, due to the lack of the fragmentation functions, we do not plot the fragmentation contribution for Ξ and Ω . Because of the difference in beam energy, the model overestimates the yields of $\Lambda + \Sigma^0$, Ξ^- , Ω^- , and their antiparticles, and the discrepancy is larger for a larger number of strange quarks in a given baryon.

B. Yield Ratios

One of the most interesting data from RHIC is the yield ratio of protons(or antiprotons) to pions at the intermediate transverse momentum region ($2 < P_T < 5$ GeV) in central heavy-ion collisions. The p/π and \bar{p}/π ratios rise steeply with P_T up to about 2.5 GeV, but levels off at about 1 and 0.7, respectively, in $2.5 < P_T < 5$ GeV for the most central 10 % Au + Au

collisions [24, 31]. At $P_T > 2$ GeV, p/π and \bar{p}/π for peripheral collisions are similar to those for elementary $p + p$ and e^+e^- collisions, and the ratios increase from peripheral to central collisions. Since the hydrodynamic model, which had been rather successful in describing the low P_T hadron spectra, could not explain the centrality dependence of limiting values, a recombination mechanism of hadronization at intermediate P_T was proposed as a possible resolution [8]. The recombination process naturally explains that the p/π and \bar{p}/π ratios level off in $2 < P_T < 5$ GeV, and fall sharply near $P_T \simeq 5$ GeV where the fragmentation takes over the recombination. Similar trends can also be found in the present calculation. The top row of Fig. 6 shows the results from our calculations for the p/π^0 , \bar{p}/π^0 , and \bar{p}/p ratios in comparison with the published PHENIX data [24]. As P_T increases, the p/π^0 and \bar{p}/π^0 ratios rises, reach the maximum values around 3 GeV, decrease sharply, and, finally, become constant at about 0.1 for $P_T > 6$ GeV. In addition, the \bar{p}/p ratio is almost constant at about 0.9 for $P_T < 5$ GeV. However, it also decreases with P_T , and become almost constant at about 0.1 for $P_T > 7$ GeV, which is very different from the previous calculation by Fries *et al.* (the dashed line in Fig. 6) [8]. Such a difference at high P_T must come from the fact that incident heavy ions possess valence quarks, but not antiquarks. In other words, the charge conjugation symmetry is already broken in RHIC environment due to the initial nuclei carry only nucleons (not antinucleons). Since the baryon number (or, equivalently, the quark number) must be conserved through the reactions, more protons than antiprotons are expected in the fragmentation region.

For more comparisons on the hadron yield ratios, the bottom row of Fig. 6 shows K^+/π^+ , K^-/π^- , and K^-/K^+ . Although the measured P_T range of K^\pm is limited, the present estimates are in reasonable agreements with the data. The K^+/π^+ and K^-/π^- ratios increase with P_T , and reach maximum around $P_T = 3$ GeV. If P_T further increases, K^+/π^+ and K^-/π^- decrease, and level off at some constants. The P_T dependence of the K^-/K^+ ratio is very similar to that of \bar{p}/p . Especially, we note that the present results on K^-/π^- and K^-/K^+ at high P_T region, where the fragmentation is dominant, are quite different from the previous model calculations by Fries *et al.* [8]. This difference also comes from different treatment of the fragmentation function like the \bar{p}/p ratio. The forthcoming RHIC data at high P_T , e.g., the PHENIX data with newly installed aerogel detector, can resolve the ambiguity.

C. Nuclear Modification Factors

Another important feature of the RHIC data can be identified in the nuclear modification factor R_{CP} , which is defined by the N_{coll} scaled central to peripheral yield ratios:

$$R_{CP} = \frac{Yield^{central} / \langle N_{coll}^{central} \rangle}{Yield^{peripheral} / \langle N_{coll}^{peripheral} \rangle}. \quad (13)$$

The RHIC experiments observed that the R_{CP} parameters of various mesons in $P_T > 2$ GeV in central collisions were suppressed with respect to the N_{coll} scaled $p + p$ and peripheral collision data. Moreover, the suppression in the intermediate transverse momentum region ($2 < P_T < 4$ GeV) was only for mesons, but not for baryons. The experimental R_{CP} parameter of protons in intermediate transverse momentum region is unity, which is completely consistent with N_{coll} scaling. The R_{CP} of Λ and $\bar{\Lambda}$ are also close to unity in an intermediate P_T region, but somewhat smaller than protons.

One of possible explanations for the suppression of hadron yields at high P_T and a distinguished behavior of mesons and baryons at the intermediate P_T region is the combined effect of recombination and fragmentation. Figure 7 shows the estimated R_{CP} parameters of π , p , and $\Lambda + \bar{\Lambda}$ as a function of P_T . For pions, we plot charged and neutral pions together, as almost no difference is expected from the present model. In the model calculation, one additional assumption was that the ratio of the volume for the parton source in peripheral to that in central collisions was about 40 % of the number of participant (N_{part}) ratio:

$$\frac{V^{peripheral}}{V^{central}} = c \frac{N_{part}^{peripheral}}{N_{part}^{central}}, \quad (14)$$

where $c = 40$ % fitted by the R_{CP} parameters of π , p , and $\Lambda + \bar{\Lambda}$, simultaneously. This is, qualitatively, understandable as the flow velocity is larger for more central collisions. The agreement between the present calculations and the experimental data are reasonable for all considered hadron species.

IV. CONCLUSIONS

We have presented an extended formalism of the recombination model to analyze the effects from the variation of the hadron's light-front wavefunctions. Two different functional forms of the light-front wavefunction, which are the Gaussian form and the power-law

form, are tested in detail. The hadron spectra are indeed sensitive to the shape of the wavefunctions. However, when we fit the wavefunction parameters to the physical observables, such as the average charge radius, the final spectra are very similar each other. We discuss our numerical results in comparison with the published RHIC data, especially, from the PHENIX and STAR collaborations. In the hadron spectra, the recombination of thermal partons dominates at the intermediate transverse momentum region between 2 and 5 GeV, and the fragmentation dominates at high P_T larger than 5 GeV. The yield ratios and the nuclear modification factors for various hadron species are also estimated. In general, the present model, which combines the recombination and fragmentation processes, are quite consistent with the experimental data. We present new predictions on \bar{p}/p and K^-/K^+ ratios, including the jet quenching effects to the fragmentation mechanism.

Acknowledgments

This work is supported in part by a grant from the U.S. Department of Energy(DE-FG02-96ER40947) and a brain pool program from the KOFST. CRJ thanks to the faculty and staff at the School of Physics at Seoul National University for the hospitality during the Sabbatical visit while this work was made.

- [1] T. D. Lee, Nucl. Phys. **A750**, 1 (2005).
- [2] I. Arsene *et al.*, BRAHMS Collaboration, Nucl. Phys. **A757**, 1 (2005).
- [3] K. Adcox *et al.*, PHENIX Collaboration, Nucl. Phys. **A757**, 184 (2005).
- [4] B. B. Back *et al.*, PHOBOS Collaboration, Nucl. Phys. **A757**, 28 (2005).
- [5] J. Adams *et al.*, STAR Collaboration, Nucl. Phys. **A757**, 102 (2005).
- [6] X. N. Wang, Phys. Rev. C **63**, 054902 (2001).
- [7] M. Gyulassy, I. Vitev, and X. N. Wang, Phys. Rev. Lett. **86**, 2537 (2001).
- [8] R. J. Fries, B. Müller, C. Nonaka, and S. A. Bass, Phys. Rev. C **68**, 044902 (2003); Phys. Rev. Lett. **90**, 202303 (2003).
- [9] D. Molnár and S. Voloshin, Phys. Rev. Lett. **91**, 092301 (2003).
- [10] V. Greco, C. M. Ko, and P. Levai, Phys. Rev. C **68**, 034904 (2003).

- [11] T. S. Biro, P. Levai, and J. Zimanyi, Phys. Lett. B **347**, 6 (1995).
- [12] P. Csizmadia and P. Levai, J. Phys. G **28**, 1997 (2002).
- [13] B. Hong, J. Korean Phys. Soc. **45**, L795 (2004).
- [14] A. Andronic, P. Braun-Munzinger, K. Redlich, and J. Stachel, Phys. Lett. B **571**, 36 (2003).
- [15] H.-M. Choi and C.-R. Ji, Phys. Rev. D **56**, 6010 (1997).
- [16] C.-R. Ji and S. R. Cotanch, Phys. Rev. D **41**, 2319 (1990).
- [17] F. Schlumpf, Phys. Rev. D **50**, 6895 (1994).
- [18] D. K. Srivastava, C. Gale, and R. J. Fries, Phys. Rev. C **67**, 034903 (2003).
- [19] B. A. Kniehl, G. Kramer, and B. Pötter, Nucl. Phys. **B582**, 514 (2000).
- [20] D. de Florian, M. Stratmann, and W. Vogelsang, Phys. Rev. D. **57**, 5811 (1998).
- [21] R. Baier, Y. L. Dokshitzer, A. H. Müller, and D. Schiff, J. High Energy Phys. **0109**, 033 (2001).
- [22] B. Müller, Phys. Rev. C **67**, 061901 (2003).
- [23] S. S. Adler *et al.*, PHENIX Collaboration, Phys. Rev. Lett. **91**, 072301 (2003).
- [24] S. S. Adler *et al.*, PHENIX Collaboration, Phys. Rev. C **69**, 034909 (2004).
- [25] S. S. Adler *et al.*, PHENIX Collaboration, Phys. Rev. C **72**, 014903 (2005).
- [26] J. Adams *et al.*, STAR Collaboration, Phys. Rev. Lett. **92**, 112301 (2004).
- [27] J. Adams *et al.*, STAR Collaboration, Phys. Lett. B **612**, 181 (2005).
- [28] K. Adcox *et al.*, PHENIX Collaboration, Phys. Rev. Lett. **89**, 092302 (2002).
- [29] C. Adler *et al.*, STAR Collaboration, Phys. Rev. Lett. **89**, 092301 (2002).
- [30] J. Adams *et al.*, STAR Collaboration, Phys. Rev. Lett. **92**, 182301 (2004).
- [31] S. S. Adler *et al.*, PHENIX Collaboration, Phys. Rev. Lett. **91**, 172301 (2003).

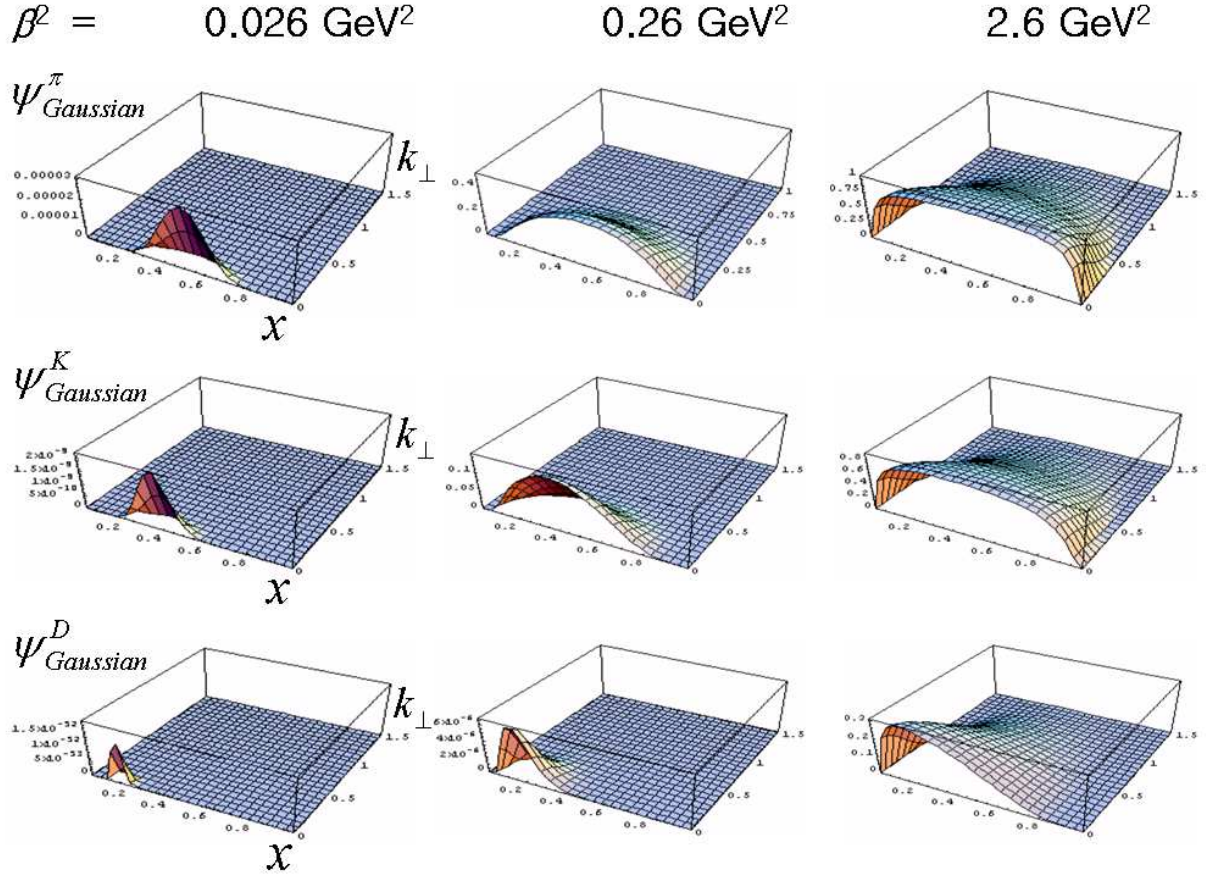


FIG. 1: Shape of the Gaussian wavefunction as functions of x and k_{\perp} for different β^2 (normalization is not performed in this figure). The top, middle, and bottom rows represent the wavefunctions for π , K , and D , respectively.

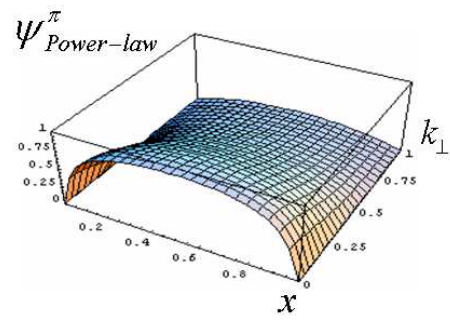
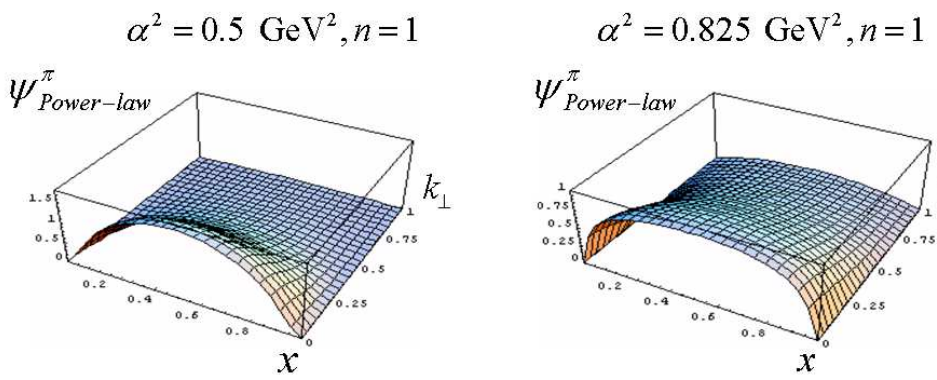
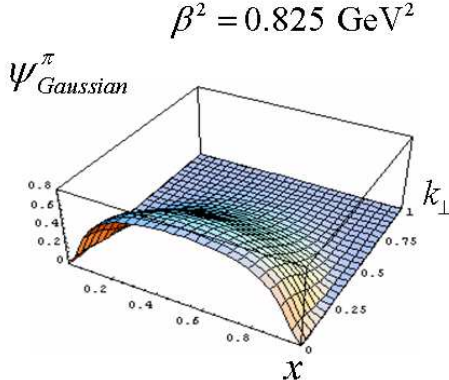


FIG. 2: Comparison of the pion wavefunctions between the Gaussian form and the power-law form. The Gaussian wavefunction with $\beta^2 = 0.825 \text{ GeV}^2$ (top) and the first order power-law wavefunction with $\alpha^2 = 0.5 \text{ GeV}^2$ (bottom left) are adjusted to the average charge radius of pions. But the power-law wavefunction with $\alpha^2 = 0.825 \text{ GeV}^2$ (bottom right) is not adjusted.

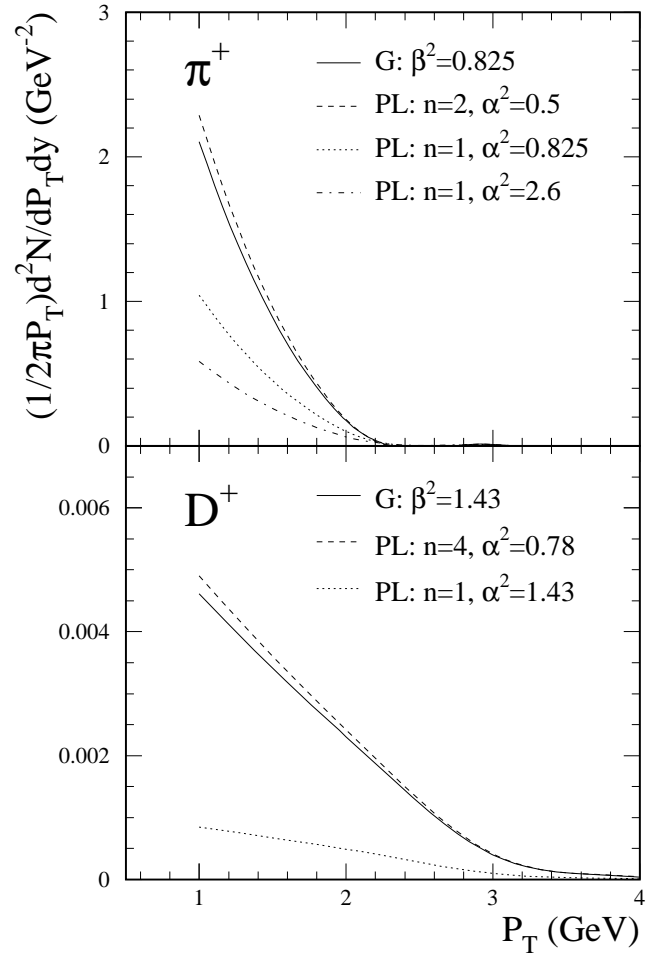


FIG. 3: Comparison of the invariant spectra of π^+ (top) and D^+ (bottom) from the recombination for various assumptions on the wavefunction parameters. G and PL represent the Gaussian and the power-law wavefunctions, respectively.

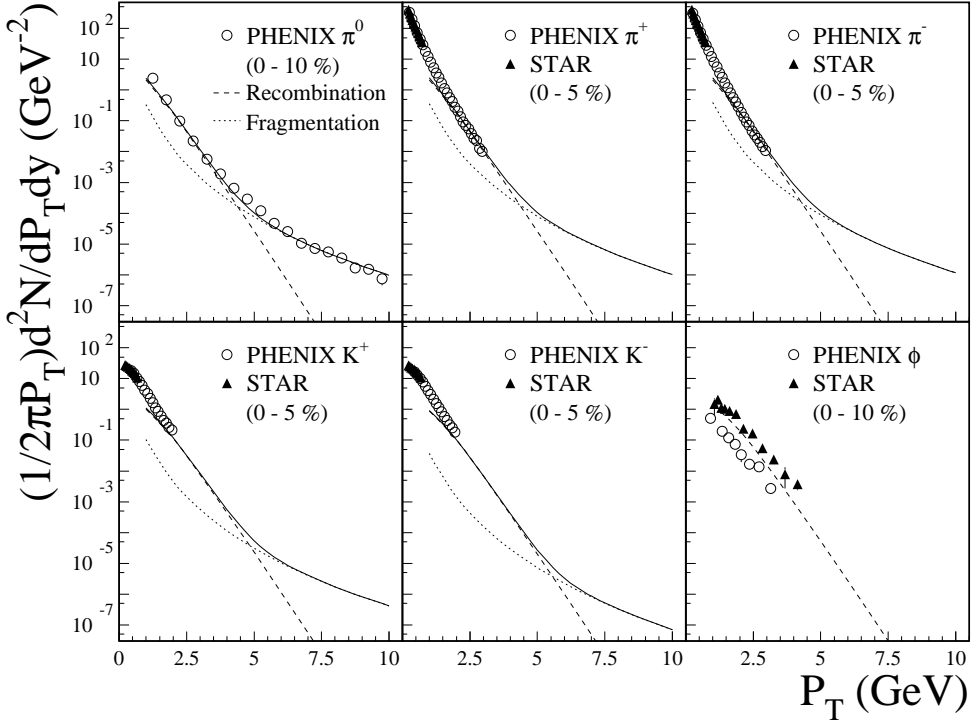


FIG. 4: Invariant spectra of mesons at midrapidity for central Au + Au collisions at $\sqrt{s_{NN}} = 200$ GeV. The dashed and dotted lines represent the model calculations from the recombination and the fragmentation, respectively. The solid lines are the sum of two contributions. The open circles are the published data by the PHENIX collaboration [23, 24, 25], and the solid triangles are those by the STAR collaboration [26, 27].

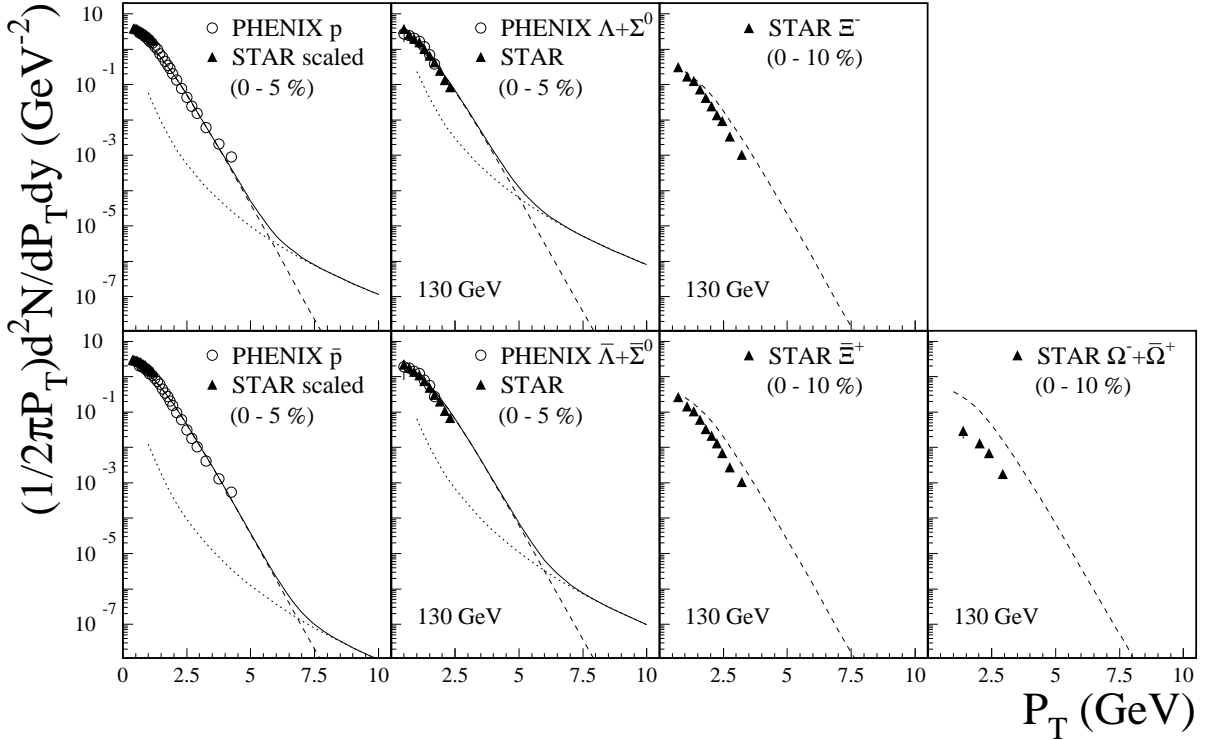


FIG. 5: Invariant spectra of baryons at midrapidity for central Au + Au collisions at $\sqrt{s_{NN}} = 200$ GeV. The dashed and dotted lines represent the model calculations from the recombination and the fragmentation, respectively. The solid lines are the sum of two contributions. The open circles are the published data by the PHENIX collaboration [24, 28] whereas the solid triangles are those by the STAR collaboration [26, 29, 30]. For a fair comparison between two sets of the data, the published p and \bar{p} spectra by the STAR collaboration [26] are scaled by 0.6, which removes the contribution by the weak decays of Λ , Σ^0 , and their antiparticles. Note that the experimental invariant spectra of hyperons are for $\sqrt{s_{NN}} = 130$ GeV, whereas all model calculations are for $\sqrt{s_{NN}} = 200$ GeV.

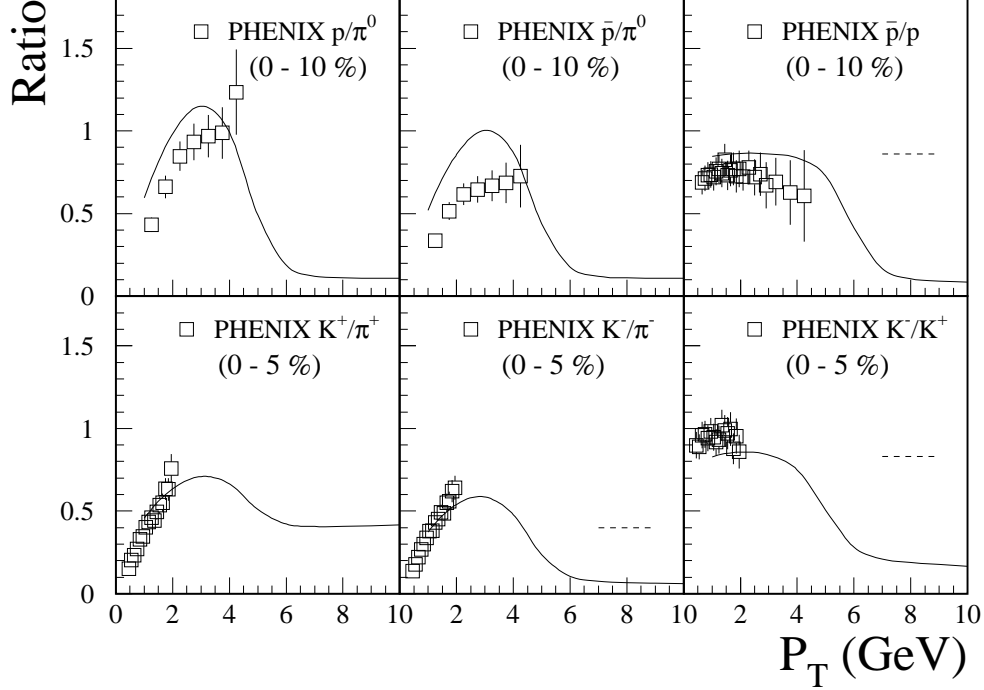


FIG. 6: Calculated hadron yield ratios (solid lines) as a function of P_T in comparison with the PHENIX data [24]. For the comparison, we also show the model calculations by Fries *et al.*, in \bar{p}/p , K^-/π^- , and K^-/K^+ by dashed lines [8].

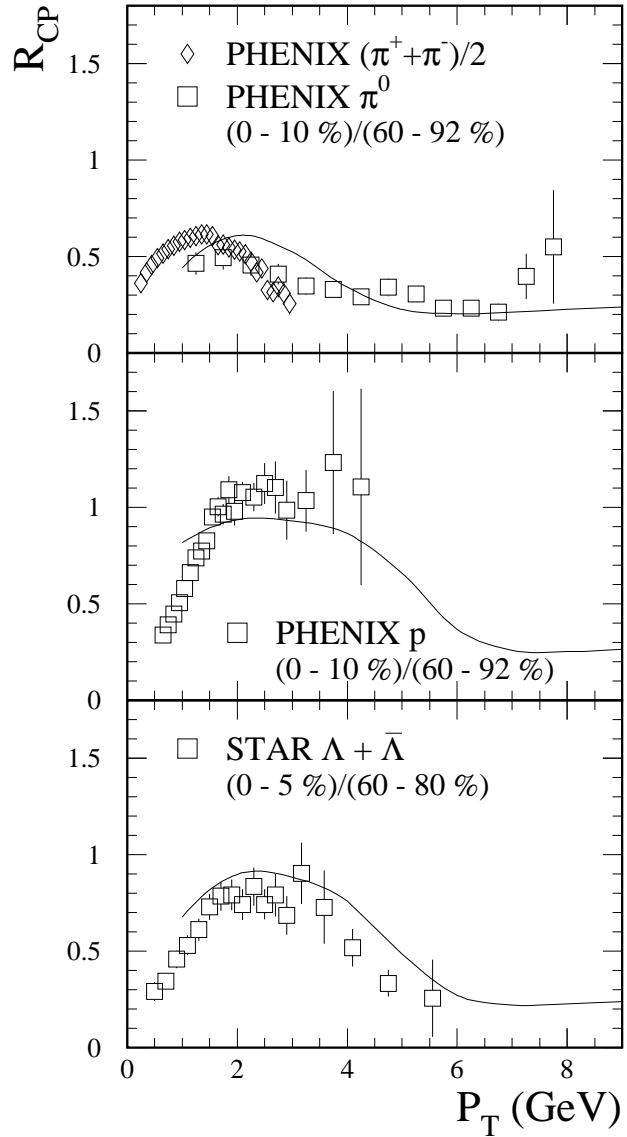


FIG. 7: Nuclear modification factors R_{CP} as a function of P_T for π , p , and $\Lambda + \bar{\Lambda}$. The solid lines are from the present calculation.